Synthesis conditions of porous clay heterostructure (PCH) optimized for volatile organic compounds (VOC) adsorption

Philje Yang*, Mugeun Song*, Daekeun Kim*, Sokhee Philemon Jung**, and Yuhoon Hwang*,†

*Department of Environmental Engineering, Seoul National University of Science and Technology, Seoul 01811, Korea
**Department of Environment and Energy Engineering, Chonnam National University, Gwangju 61186, Korea

Abstract−Volatile organic compounds (VOCs) can cause carcinogenic risk, odor problems, and even generation of particulate matter. Adsorption is an effective technique for controlling VOC emissions at the source. In this study, porous clay heterostructure (PCH) was considered as a possible VOC adsorbent, and the synthesis conditions were optimized. The ratio of tetraethyl orthosilicate (TEOS) compared to organoclay and dodecylamine (DDA) was selected as a synthesis condition variable (organoclay : dodecylamine : TEOS=1 : 1 : 30-120). We investigated the change of morphology and porosity of PCH by using a transmission electron microscope, nitrogen adsorption/desorption, and x-ray fluorescence. The porosity of PCH was changed depending on the TEOS ratio. As the ratio of TEOS decreased, the pore size of the PCH also decreased. However, irregular layer expansion was observed due to the swelling of organoclay by DDA in PCH30. To evaluate the possibility of using PCH as an adsorbent for low concentration VOCs, specifically toluene and decane, adsorption experiments were conducted, and it was confirmed that micropores play an essential role for low concentration VOC adsorption. PCH60 was selected as an optimal condition. The toluene and decane adsorption capacity of PCH60 was, respectively, measured as 122.92 mg/g and 886.73 mg/g.

Keywords: PCH, Adsorption, VOC, TEOS, Micropore

INTRODUCTION

The US EPA defines volatile organic compounds (VOCs) as organic compounds having vapor pressure exceeding 0.1 mm Hg at standard conditions. Since VOCs with high vapor pressure exist as the gas phase and can diffuse quickly, they pose a high risk to human health [1]. For example, benzene and styrene are regulated because they cause cancer and odor problems [2,3]. Moreover, VOCs in the air are transformed into secondary atmospheric particulate matter (PM) through photochemical reactions, resulting in serious environmental problems. It was reported that 20-50% of the PM was found to be organic substances in the mid-latitudes and up to 90% in the tropical areas [4]. Primarily, toluene and benzene are known as the main VOCs that contribute to secondary PM formation [5]. In Korea, 50-70% of the secondary PM is derived from organic compounds, with toluene reported as the primary organic PM precursor, accounting for 54.5% of organic PM precursor. Therefore, the management of VOCs is becoming more critical in order to mitigate air pollution by PM [6].

As VOCs are discharged into the gas phase and diffuse quickly, treatment at the source is more important than treatment after they are discharged into the air. Because the recovery or treatment of diffused VOCs in the air is almost impossible, it is necessary to develop a VOC treatment technology that can be applied at the VOC source. Various techniques, such as the use of biofilters [7], bio-

scrubbing [8], catalytic oxidation [9], heating oxidation [10], and adsorption [11], have been utilized to control VOCs at the source. Adsorption has been successfully applied in commercial systems because of its easy operation and ability to treat mixed gas [12]. Adsorption with activated carbon is the most common technique. Low price and high adsorption performance have led to the use of activated carbon [13]. However, low regeneration efficiency and vulnerability to fire are problems that reduce the applicability of activated carbon [14-16]. Among various VOC emission sources, there are several places where it is challenging to apply activated carbon because of high temperature, such as dry cleaners. The dry cleaner is a good example where VOC recovery is necessary. It discharges a large amount of solvent that is used for dry cleaning. The high-temperature gas discharged from the dryer makes it challenging to apply activated carbon. To manage VOCs, it is necessary to develop an adsorbent that can be applied to high-temperature gas.

Clay mineral, which is a natural resource easily obtained in soil, is inexpensive with abundant reserves and has a unique molecular structure. Due to its interlayer space between the plate layers and cation exchange capacity, it has been used as an adsorbent for heavy metals, organic compounds, and humic acid [17-19]. There have been extensive efforts to use low-cost clay minerals as VOC adsorbents, but the adsorption capacity at low concentration VOCs is about only 10% of that of activated carbon [20]. To improve the adsorption performance of clay, various attempts have been made to expand the interlayer space between plates [21,22]. Organoclay [23] and pillared clay [24] are well-known examples to utilize the interlayer space of clay minerals. Porous clay heterostructure (PCH) is a kind of pillared clay that creates silicon pillars in the interlayer

space of clay to obtain empty pores. PCH has the potential to be used as a VOC adsorbent because it has much better pore development than other materials based on clay minerals. Synthesis of PCH was accomplished by mixing organoclay and expanding the interlayer space of clay minerals with organic materials, tetraethyl orthosilicate (TEOS) and dodecylamine (DDA), to form silicon pillars. DDA is a co-surfactant that fills the interlayer of organoclay and reacts with TEOS to form silicon pillars. The mixture is finally calcined at 550 °C to remove organic matter. In this process, the silicon pillars remain and the space where the organic materials were becomes empty pores [25].

PCH has a large surface area and large pore volume as the interlayer space is expanded by silicon pillars. Since the pores act as an adsorption space, the larger the pore volume is, the better the adsorption performance will be. In particular, PCH developed micropores because the pores are formed in the narrow interlayer space. The micropores have the advantage of adsorbing low concentration VOCs [26]. To eliminate the emission of VOCs, the adsorbent should be able to treat low concentration VOCs, and thus the presence of micropores is the main parameter determining adsorption performance. In addition to the pore structure, PCH has another advantage that facilitates application to VOC adsorption in dry cleaners. The main component of PCH is Si, which has the advantage of excellent heat resistance. Therefore, it will be possible to apply it to high-temperature emission gases from dry cleaners [15,27]. However, there are still limitations to the application of PCH. The amount of TEOS for PCH synthesis is generally required to be over 120-times the weight of the organoclay. This excessive TEOS amount required for PCH synthesis makes it expensive. Moreover, it was reported that the pore structure of PCH is affected by the ratio of TEOS [28]. The change of pore structure was investigated with the TEOS ratio in a range of 20-80. When the TEOS ratio was as low as 20 times of the organoclay, a partially delaminated structure was observed due to the inhomogeneous dispersion of the reaction system and the swelling and solvation effect of DDA. The pore structure plays a vital role in adsorption performance, and thus the synthesis ratio for the adsorbent should be optimized. However, the effect of the TEOS ratio on VOC adsorption has not been reported thus far.

In this study, the ratio of TEOS was optimized in order to minimize the overall production cost as well as maximize the adsorption capacity. As the model PCH application scenario, a dry cleaner that emitted high-temperature VOC gas was selected. Decane and toluene were chosen as the representative VOCs of alkene and aromatic groups, considering the emission amount from the dry cleaner and the contribution of PM [6,29]. The adsorption performance of PCH with different TEOS ratios was confirmed by isothermal adsorption/desorption experiments. X-ray fluorescence spectrometer (XRF), nitrogen adsorption/desorption, and transmission electron microscopy (TEM) analyses were performed to confirm the chemical structure of PCH with the TEOS ratio.

<div align="center">METHOD</div>

1. Materials

Bentonite (Sigma Aldrich) was selected as a model clay mineral for further PCH synthesis. The chemical composition of the bentonite was Si 42.35%, Al 24.75%, Mg 15.8%, Fe 8.51%, K 5.20%, Ca 2.89%, Ti 0.26%, Sr 0.09%, Zr 0.06%, Ba 0.03%, and Zn 0.02%, and the cation exchange capacity (CEC) of bentonite was reported as 110 mmol/100 g [30]. Hexadecylammonium chloride (HDTMA, >99%), tetraethyl orthosilicate (TEOS, >99.0% (GC)), and dodecylamine (DDA, 98%) were purchased from Sigma Aldrich. Decane (99+%) was purchased from Acros Organics. Toluene gas (1,000 ppm calibration gas mixtures, base gas: N_2) was purchased from Air Korea.

2. Synthesis of PCHs

The organoclay was synthesized by mixing HDTMA and bentonite. The amount of HDTMA was equal to the CEC of bentonite. The mixture was stirred for 24 h at 60 °C. The product was then separated from the solution and washed eight times with distilled water to remove residual organics. The organoclay was dried for 24 h at 60 °C and ground to pass a 35 mesh sieve.

The PCH was synthesized by mixing the aforementioned organoclay with DDA and TEOS in a weight ratio of 1 : 1 : X (X=30, 60, 90, 120; TEOS) and stirring them for 4 h. After reactions, the mixtures were separated with a centrifuge for 15 min at 3,000 rpm. The separated solid was dried at 60 °C for 24 h, and it was further calcined at 550 °C for 6 h (temperature rise 3 °C/min). The calcination was performed to remove organic matter. In this process, the silicon pillars remain and the space where the organic materials were becomes empty pores. PCH was ground with a mortar, and 150 μm-500 μm particles were collected for further analysis and tests.

3. PCHs Characterization

An X-ray fluorescence spectrometer (XRF, ARL QUANT'X, Thermo Fisher Scientific, USA) was used to determine chemical composition. The N_2 adsorption/desorption isotherms were measured at −196 °C with a 3flex (Micromeritics, USA). The sample was degassed at 150 °C for 12 h before N_2 adsorption/desorption measurements were performed. The surface area (S) was calculated using the Brunauer-Emmett-Teller (BET) equation, mesopore volume (V_{meso}) was calculated using the Barrett-Joyner-Halenda (BJH) equation, and micropore volume (V_{micro}) using the t-plot method. The average pore diameter (APD) was obtained by using BET for total pores and BJH for the mesopores. A high-resolution transmission electron microscope (HRTEM, JEM-3010, JEOL Ltd., Japan) was used to observe the morphology of the adsorbent. Before measurement, the samples were dispersed in ethanol and dropped on a copper grid.

4. VOC Adsorption/Desorption Isotherm

VOC adsorption/desorption experiments were conducted at 25 °C. 0.3 g of adsorbent was placed into the column. For the toluene adsorption test, 1,000 ppm of toluene gas flowed into the chamber at a flow rate of 300 mL/min for 30 min before the adsorption experiment was conducted. After the concentration of the chamber was stable, the adsorption experiment was conducted by flowing the gas in the chamber to the column. The emission gas was then measured by gas chromatography equipped with a flame ionization detector (GC/FID, YL6500 GC, Youngin, South Korea) every 3 min. The measurement conditions of GC/FID were as follows: oven temperature of 200 °C, flow rate of 3 mL/min, split ratio of
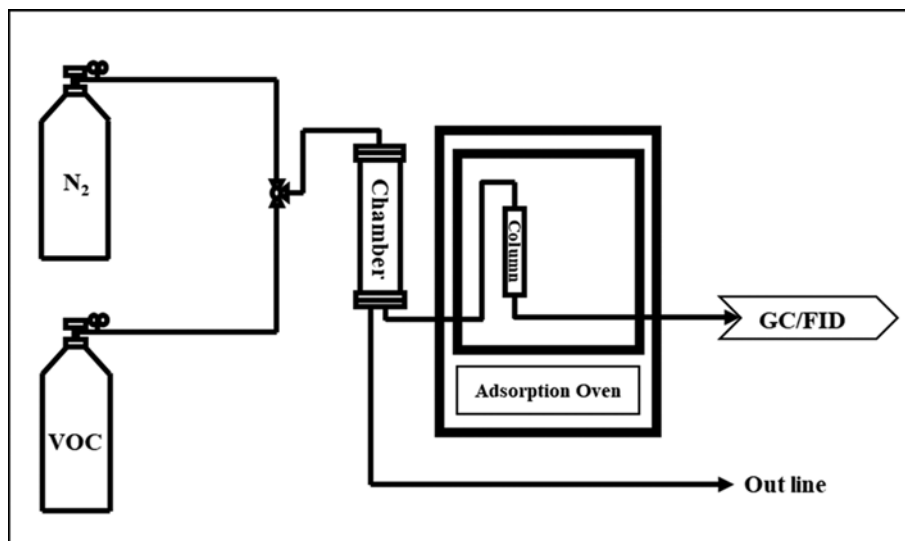
Fig. 1. Adsorption/desorption equipment schematic.

5 : 1, and FID temperature of 250 °C. In the case of the decane adsorption test, the decane gas was prepared by mixing 300 mL/min of decane saturated gas and 200 mL/min of N_2 gas.

Desorption of the adsorbent proceeded with N_2 gas purge. The chamber was purged with N_2 gas for 30 min with 300 mL/min to remove residual VOCs. The pure N_2 gas in the chamber then flowed to the column. The emission gas was measured by GC/FID at the same conditions of adsorption.

RESULTS AND DISCUSSION

1. High-resolution Transmission Electron Microscopy (HRTEM) Analysis

The structures of the clay materials were analyzed by HRTEM. Fig. 2(a) shows the structure and the interlayer space of pure bentonite. The sheet-like structure was observed as black lines, and the interlayer space existed between the black lines as white space. The
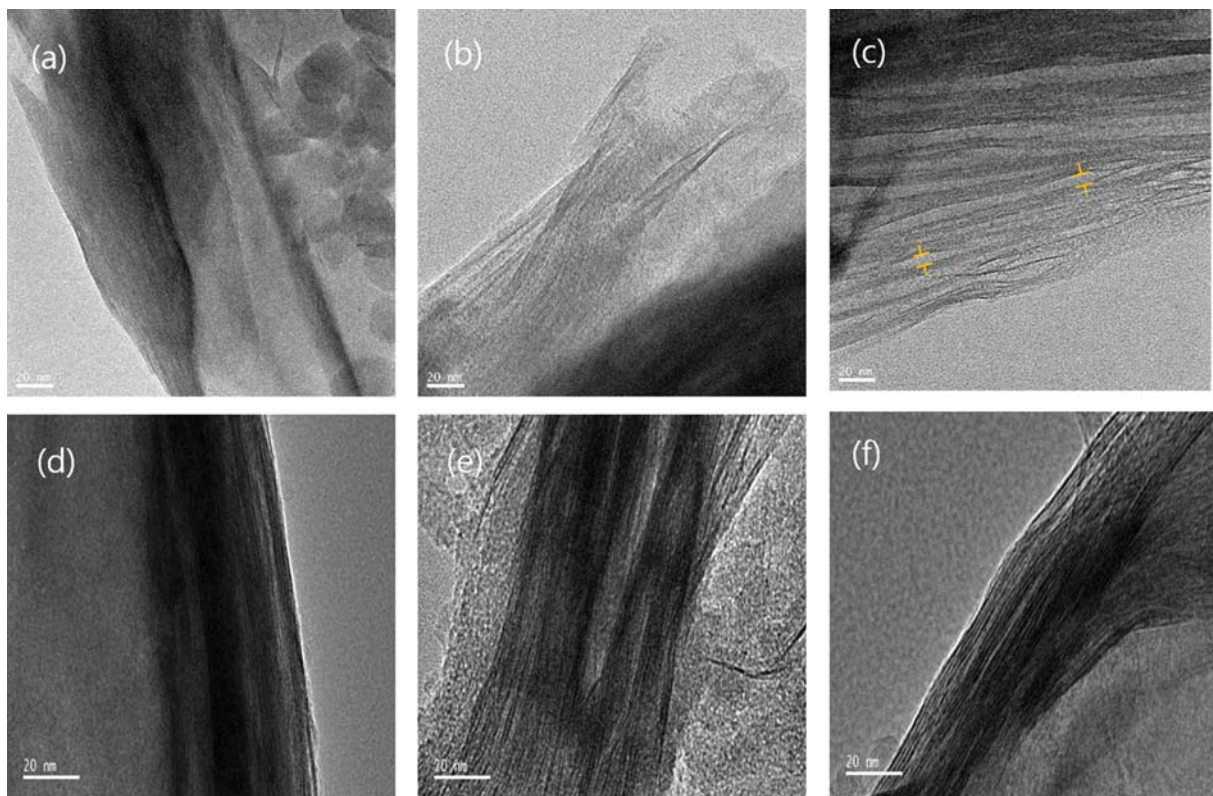

Fig. 2. TEM images of (a) Bentonite (Bt), (b, c) PCH30, (d) PCH60, (e) PCH90, (f) PCH120.

PCH interlayer space in Fig. 2(b)-(f) was more clearly visible, indicating expansion of the interlayer space.

Interestingly, the interlayer space of PCH30 was irregular, as indicated in Fig. 2(c). This characteristic was only identified in PCH30 but not in other PCHs. Therefore, the low ratio of TEOS may play an essential role in the formation of irregular interlayer space. As the amount of TEOS decreased, the concentration of DDA became relatively higher. When the intermolecular attraction exceeded the dispersion of the organic materials (DDA-TEOS), the organic matter would aggregate. The aggregated organic matter would not be located homogeneously in the clay interlayer space, and thus large pores are formed.

Similar irregular interlayer spacing at a low TEOS ratio was already reported in a study focused on PCH pore structure development [28]. Highly disordered staking, even partial delamination, was frequently observed when the TEOS ratio was 20 in a previous study. With such a small amount of TEOS, organoclay and DDA could not thoroughly disperse homogeneously, and thus part of the organoclay was highly swelled and solvated by DDA [28]. Moreover, aggregation of clay mineral was also observed in Fig. 2(b). The overlapped clay layers are found in Fig. 2(b). This was similar to a previous study that DDA can aggregate 1-4 μm of clay particles into large particles of 200 μm [31].

2. Nitrogen Adsorption/Desorption Analysis

Nitrogen adsorption/desorption experiments were performed to investigate the pore structure of clay mineral materials. Table 1 shows the pore characteristics of bentonite and prepared PCHs. Comparing the porosity of bentonite with that of PCHs, it can be seen that the porosity of PCHs was enhanced considerably. The pore volume of bentonite was measured as 0.094911 cm^3/g, while 0.302305-0.336166 cm^3/g total volume was obtained in PCHs. Notably, the micropore volume increased by 15-30 times depending on the type of PCH. In addition to the pore volume, the average pore diameter was also significantly decreased. The average pore diameter of bentonite was 88.363 nm, but it decreased to 24.25-36.31 nm in PCH. These results indicate that the micropores were produced at the interlayer space of bentonite.

It is known that the micropores are directly related to the low-concentration VOC adsorption performance, and thus the micropores of PCH are expected to contribute to lowering the VOC emission concentration [26]. The adsorption performance of the adsorbent presents differently depending on the experimental method. In the dynamic adsorption similar to the actual adsorption state, the adsorption amount is related to the micropore volume [32].

Therefore, a significant increase in micropore volume in PCHs would lead to better VOC adsorption performance.

On the other hand, the tendency of pore development at different TEOS ratios was not consistent. For example, the average pore diameter (APD) of the sample decreased with a decreasing amount of TEOS but increased in PCH30. The total pore volume (V) increased from PCH120 to PCH60 but decreased in PCH30. The tendencies of PCH120, PCH90, and PCH60 are different from those of PCH30. It appears that the dominant influence on the pore structure differed depending on the TEOS ratio.

PCH60 has a significant increase in micropore volume compared to PCH120, PCH90. However, the total pore volume of PCH120, PCH90, and PCH60 was not substantially changed. However, the portion of mesopore volume decreased, and that of micropore volume increased at PCH60. The average pore diameter was reduced as the amount of TEOS decreased. The number of pores formed was similar, but as the diameter of the mesopores decreased, they became micropores, which led to an increase in the micropore volume of PCH60. In this light, it could be surmised that the mesopores turned into micropores as the TEOS ratio was lowered from 120 to 60 in the PCH synthesis.

The pore characteristics of PCH30 were different from those of PCH120, PCH90, and PCH60. In PCH30, the total pore volume and micropore volume decreased, and the mesopore volume and pore average diameter increased. This appears to be related to the irregular interlayer space observed in Fig. 2(b)-(c). As the amount of TEOS reduced, the organic materials became aggregated, and some part of the interlayer space swelled. As a result, large pores were formed at the site where the micropores were. The amount of micropores was consequently reduced, and the mesopores increased again.

Fig. 3 shows a nitrogen adsorption/desorption graph of bentonite and PCHs. It can be confirmed that the adsorption performance of PCHs was improved compared to bentonite. While PCH120, PCH90, and PCH30 had similar initial adsorption, high initial adsorption of PCH60 was measured. The higher adsorption capacity at low relative pressure was ascribed to the development of micropores in PCH60. The final adsorption capacity of PCHs was similar regardless of the TEOS ratio. The desorption graph of all materials shows a rapid desorption section at relative pressure of around 0.5. This is a phenomenon that occurs in materials with narrow and long pore-like interlayer space [33].

3. X-ray Fluorescence Spectrometer Analysis

The chemical composition of the adsorbent was measured by

Table 1. Pore analysis results for bentonite and PCHs

Sample	S (m^2/g)	V$_{total}$ (cm^3/g)	V$_{meso}$ (cm^3/g)	V$_{micro}$ (cm^3/g)	APD$_{total}$ (Å)	APD$_{meso}$ (Å)
Bt	42.9641	0.094911	0.086836	0.005814	88.363	134.632
PCH120	343.8191	0.312099	0.191632	0.08933	36.310	80.024
PCH90	352.5953	0.320386	0.193227	0.092562	35.176	75.436
PCH60	540.7124	0.336166	0.123439	0.186039	24.252	64.102
PCH30	372.1312	0.302305	0.16396	0.106612	31.575	71.962

*S=Surface area, V$_{total}$=Total pore volume, V$_{meso}$=Mesopore volume, V$_{micro}$=Micropore volume, APD$_{total}$=Average total pore diameter, APD$_{meso}$(A)= Average mesopore diameter
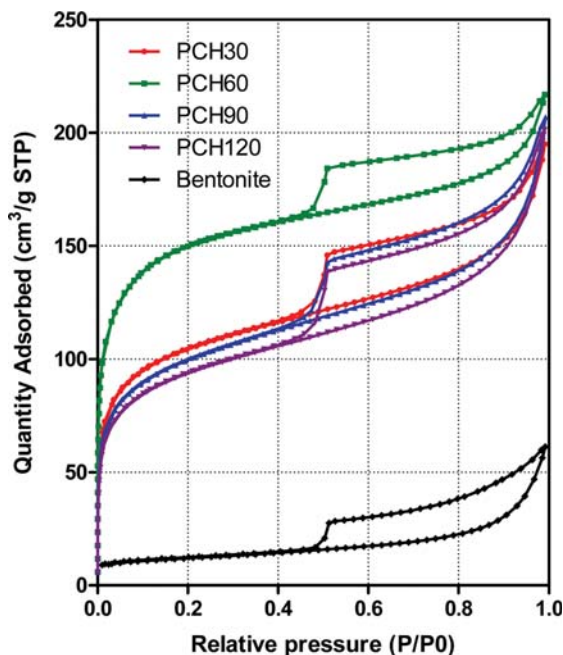
Fig. 3. Nitrogen adsorption/desorption isotherms at −196 °C for bentonite and PCHs.

Table 3. The toluene adsorption capacity of PCH

	PCH30	PCH60	PCH90	PCH120
Q_{ad} (mg/g)	92.57±2.72	122.92±5.39	72.70±0.28	74.59±3.94
Q_{de} (mg/g)	86.52±0.21	119.56±0.96	63.22±10.35	69.69±6.96
R_{de} (%)	93.51±2.97	96.81±4.24	86.86±13.63	93.27±4.47

*Q_{ad}: adsorption quantity, Q_{de}: desorption quantity, R_{de}: desorption ratio=Q_{de}/Q_{ad}

an XRF analysis. The analyzed results are presented in Table 2. The main component of the bentonite is Si 42.35%, followed by Al 24.75%, Mg 15.8%, and Fe 8.51%. Since bentonite is composed of metal-based materials, it is highly heat-resistant. Due to its high heat-resistance, clay mineral has even been used to increase the heat resistance of carbon materials [34]. The chemical composition of PCH60 is slightly different from bentonite. The ratio of silicon increased by about 10% from 42.35% of bentonite to 54.35% of PCH. This is because the silicon component of TEOS was added to bentonite as a pillar-like structure [28].

4. Toluene Adsorption/Desorption

Fig. 4(a) shows the toluene breakthrough curve of bentonite

and PCHs with different TEOS ratios. In the case of bentonite, we failed to measure the toluene adsorption performance as it broke through the first measurement after the start of adsorption (3 min). On the other hand, PCHs showed breakthrough curves indicating toluene adsorption on PCHs. The ratio of TEOS also changed the adsorption performance. The breakpoint was measured with PCH90 at 9 min, PCH120 12 min, PCH30 17 min, and PCH60 18 min. The breakpoint was selected as the point where the emission concentration exceeded 5% of the inflow concentration. The time where the breakpoint of PCH60 appeared was 1.5-times longer than that of PCH120. Desorption curves are presented in Fig. 4(b). Overall, similar desorption behaviors were shown except for longer desorption time for PCH60, which is due to a large amount of adsorbed toluene.

Table 3 summarizes the adsorption performance of PCHs in more detail. Toluene adsorption capacity was similar for PCH120 and PCH90 at 74.59 mg/g and 72.7 mg/g. PCH30 and PCH60 showed high adsorption amounts of 92.57 mg/g and 122.92 mg/g, respectively. The adsorption capacity of PCH60 increased 1.6-times as compared with that of PCH120, which is a typical reported PCH synthesis ratio [15,20]. The overall desorption performance was satisfactory. The desorption efficiency of PCH60 was determined as 96.81%. In comparison, the desorption rate of nitrogen purging of activated carbon conducted in another study was reported as 31.58% [35].

Fig. 5 shows the relationship between toluene adsorption capac-

Table 2. The chemical composition of adsorbents analyzed by XRF

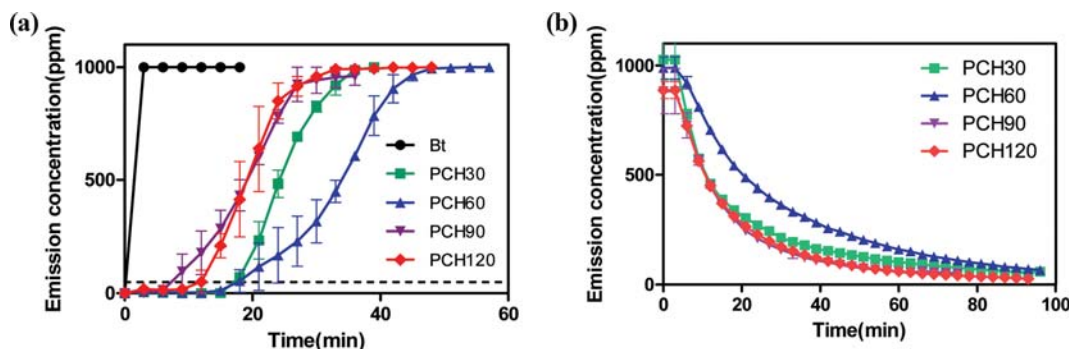|	Si (%)	Al (%)	Mg (%)	Fe (%)	K (%)	Ca (%)	Ti (%)
Bt	42.35	24.75	15.8	8.51	5.20	2.89	0.267
PCH60	54.35	17.56	17.4	5.93	3.35	1.20	0.176

Fig. 4. Toluene adsorption/desorption curves of PCHs and bentonite (a) breakthrough curves, (b) desorption curves.
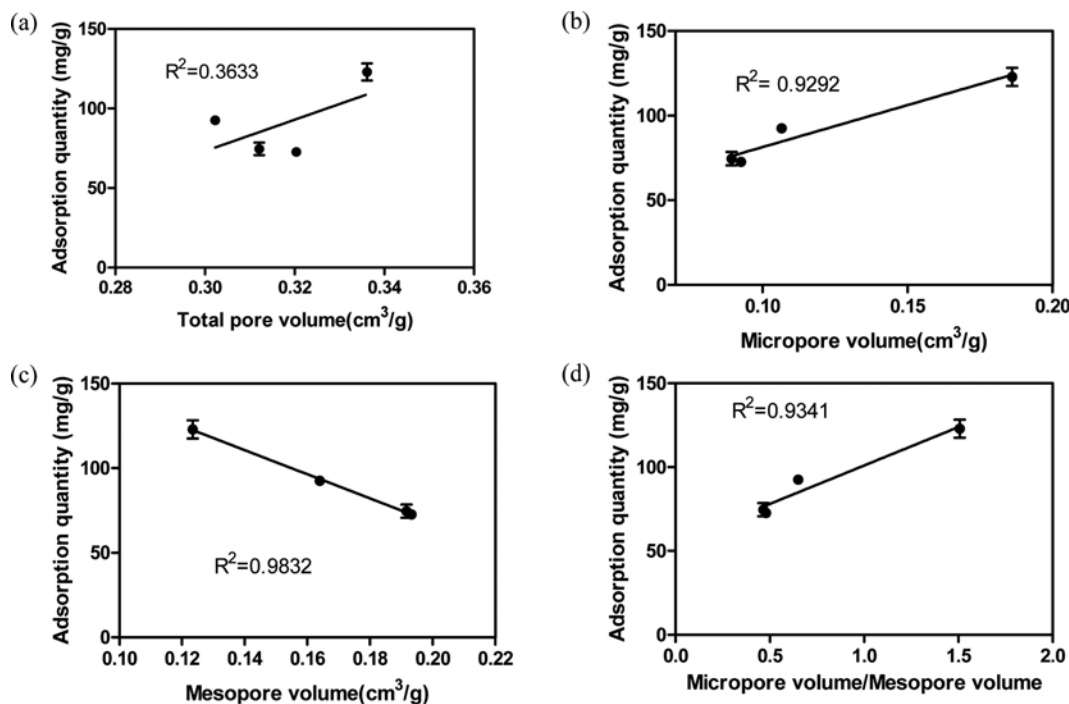
Fig. 5. Relationship between toluene adsorption quantity and pore structures, (a) total pore volume, (b) micropore volume, (c) mesopore volume, (d) micropore volume/mesopore volume.

ity and pore structure indicators, such as total pore volume, micropore volume, mesopore volume, and the ratio of micropore volume and mesopore volume. The total pore volume does not have a strong correlation with toluene adsorption (R^2=0.3633). Interestingly, the micro- and mesopore volume has a strong correlation with toluene adsorption. Mesopore volume has a negative correlation (R^2=0.9832), while micropore has a positive correlation (R^2=0.9292).

It was clear that the total pore volume does not change significantly by the change of TEOS ratio. The total pore volume of PCHs was increased around 3.19- to 3.54-times compared to bentonite. However, the generation of micropores was significantly different depending on the TEOS ratio. PCH60 has a high ratio of micropore (micropore : mesopore=1.51 : 1), while PCH120 has the lowest micropore ratio (micropore : mesopore=0.47 : 1). Therefore, the ratio of micropore volume and mesopore volume also has a strong positive correlation with toluene adsorption (R^2=0.9341). This indicates that the toluene adsorption is very closely related to the micropore volume, and is consistent with the relationship between the micropore volume and the low concentration VOC adsorption amount in another study [36].

In other studies, the maximum toluene adsorption capacity was reported as 510.46 mg/g in activated carbon, 66 mg/g in bentonite, and 58.63 mg/g in organoclay [37,38]. However, these adsorption capacities were obtained by a batch adsorption test in high relative pressure. Thus, these results cannot be directly compared with our experimental results because we used a dynamic flow-through adsorption test under low relative pressure ($0.026P/P_0$). In dynamic adsorption of toluene, the toluene adsorption capacity was reported as 87.937 mg/g in activated carbon at $0.045P/P_0$, 37.47 mg/g in silica gel at $0.045P/P_0$, and 7.920 mg/g in 13X zeolite at $0.091P/P_0$ [39].

In this regard, it could be concluded that PCH has excellent adsorption/desorption performance compared to activated carbon.

5. Decane Adsorption/Desorption on PCH60

Among the PCHs with different TEOS ratios, we chose PCH60 as an optimal adsorbent based on physical characterization and toluene adsorption results. As a model aliphatic VOC material emitted from a dry cleaner, decane was selected, and the adsorption capacity of PCH60 for decane was tested. Fig. 6 shows the dynamic adsorption/desorption graph of PCH60. The adsorption capacity of decane was 886.73 mg/g and the desorption efficiency was 40.53%. In other studies, decane adsorption experiments were carried out with various types of clay minerals. The adsorption capacity of decane was 80.24 mg/g in Ca-montmorillonite, 22.11 mg/g in an illite/smectite mixed layer, and 8.90 mg/g in kaolinite [40]. The meas-
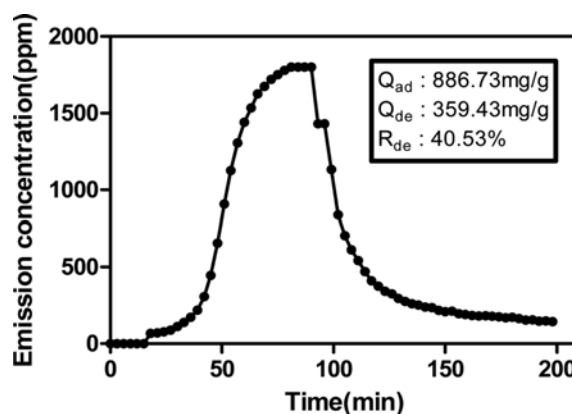

Fig. 6. Decane adsorption/desorption curve of PCH60.

ured adsorption capacity in this study was ten-times higher than the previously reported value, even though it was conducted at low partial pressure. Compared with the adsorption capacity (293.12 mg/g) of activated carbon, that of PCH was comparably higher [41].

Overall, PCH60 showed higher adsorption performance for decane, while the desorption performance was worse than that of toluene. The different adsorption/desorption results of decane compared to toluene are due to the difference in adsorption affinity toward the adsorbent. Toluene and decane have different molecular structures, and thus their behavior is different in the pores. Previous study of mixed gas (propane, toluene, and decane) adsorption experiments using zeolite as an adsorbent showed that the amount of adsorbed decane was much higher than that of toluene and propane [42]. The adsorption selectivity toward decane was explained by the different hydrocarbon characteristics and the possible adsorbent sites offered by the adsorbent.

Similar results could be found in the case of activated carbon as well. Ushiki et al. [43] reported higher decane adsorption capacity of activated carbon compared to toluene. This was explained by the characteristic adsorption energy (E; kJ/mol) derived from the Dubinin-Astakhov equation. The parameter E varied greatly between VOCs, which may be due to the difference in interaction energy between the adsorbent and VOCs. Generally, the parameter E appears to become larger with increasing molecular size. The adsorption energy of decane was reported as 17.50-18.55 kJ/mol, while the adsorption energy of toluene was reported as 11.89-16.84 kJ/mol. The higher adsorption energy of decane could be explained by the larger molar volume (195.0 cm^3/mol) compared to toluene (106.3 cm^3/mol). Due to the high adsorption energy of decane, higher adsorption capacity, as well as lower desorption efficiency, was observed in previous reports [43,44].

CONCLUSIONS

VOC adsorption experiments and structural analyses were conducted to select the optimum TEOS ratio for PCH synthesis. Structural analyses showed that the amount of TEOS had a significant effect on the pore development of PCH, especially on the size of the pore. As the quantity of TEOS decreased, the pore size of the PCH also decreased. However, an irregular interlayer space developed when the TEOS ratio was too low due to the aggregation of organic matter and swelling of organoclay.

To evaluate the possibility of using PCH as an adsorbent of low concentration VOCs, specifically toluene and decane, adsorption experiments were conducted, and it was confirmed that micropores play an essential role for low concentration VOC adsorption. PCH60 showed 1.6-times more toluene adsorption capacity than PCH120 and showed excellent adsorption performance for decane. The toluene and decane adsorption capacity of PCH60 was, respectively, measured as 122.92 mg/g and 886.73 mg/g.

PCH60 improved the economics of PCH by reducing the amount of TEOS required for a typical PCH ratio by half. However, the desorption performance differs depending on VOCs, and thus an additional desorption technique should be considered to regenerate the spent adsorbent effectively.

REFERENCES

1. Z. Shareefdeen and A. Singh, Biotechnology for odor and air pollution control, Springer Science & Business media, Berlin, Heidelberg (2005).
2. M. Tancrède, R. Wilson, L. Zeise and E. A. C. Crouch, *Atmos. Environ.*, **21**, 2187 (1987).
3. R. Iranpour, H. H. J. Cox, M. A. Deshusses and E. D. Schroeder, *Environ. Prog. Sustain. Energy*, **24**, 254 (2005).
4. M. Kanakidou, J. H. Seinfeld, S. N. Pandis, I. Barnes, F. J. Dentener, M. C. Facchini, R. Van Dingenen, B. Ervens, A. Nenes, C. J. Nielsen, E. Swietlicki, J. P. Putaud, Y. Balkanski, S. Fuzzi, J. Horth, G. K. Moortgat, R. Winterhalter, C. E. L. Myhre, K. Tsigaridis, E. Vignati, E. G. Stephanou and J. Wilson, *Atmos. Chem. Phys.*, **5**, 1053 (2005).
5. R. G. Derwent, M. E. Jenkin, S. R. Utembe, D. E. Shallcross, T. P. Murrells and N. R. Passant, *Sci. Total Environ.*, **408**, 3374 (2010).
6. H. Shin, J. Kim, S. Lee and Y. Kim, *Environ. Sci. Pollut. Res.*, **20**, 1468 (2013).
7. G. Leson and A. M. Winer, *J. Air Waste Manage. Assoc.*, **41**, 1045 (1991).
8. T. Granström, P. Lindberg, J. Nummela, J. Jokela and M. Leisola, *Biodegradation*, **13**, 155 (2002).
9. M. A. Campesi, C. D. Luzi, G. F. Barreto and O. M. Martínez, *J. Environ. Manage.*, **154**, 216 (2015).
10. B.-S. Choi and J. Yi, *Chem. Eng. J.*, **76**, 103 (2000).
11. Y. Chiang, P. Chiang and C. Huang, *Carbon*, **39**, 523 (2001).
12. A. K. Ghoshal and S. D. Manjare, *J. Loss Prevent. Proc.*, **15**, 413 (2002).
13. O. Ioannidou and A. Zabaniotou, *Renew. Sust. Energy Rev.*, **11**, 1966 (2007).
14. G. E. Strudgeon, B. J. Lewis, W. W. Albury and R. C. Clinger, *J. Water Pollut. Control Fed.*, **52**, 2516 (1980).
15. L. Zhu, S. Tian and Y. Shi, *Clay. Clay Miner.*, **53**, 123 (2005).
16. F. Delage, P. Pre and P. LeCloirec, *Environ. Sci. Technol.*, **34**, 4816 (2000).
17. F. A. Banat, B. Al-Bashir, S. Al-Asheh and O. Hayajneh, *Environ. Pollut.*, **107**, 391 (2000).
18. S. A. Khan, M. A. Khan and Riaz-ur-Rehman, *Waste Manage.*, **15**, 271 (1995).
19. K. Wang and B. Xing, *J. Environ. Qual.*, **34**, 342 (2005).
20. F. Qu, L. Zhu and K. Yang, *J. Hazard. Mater.*, **170**, 7 (2009).
21. H. He, L. Ma, J. Zhu, R. L. Frost, B. K. G. Theng and F. Bergaya, *Appl. Clay Sci.*, **100**, 22 (2014).
22. L. Deng, P. Yuan, D. Liu, F. Annabi-Bergaya, J. Zhou, F. Chen and Z. Liu, *Appl. Clay Sci.*, **143**, 184 (2017).
23. L. B. de Paiva, A. R. Morales and F. R. Valenzuela Díaz, *Appl. Clay Sci.*, **42**, 8 (2008).
24. J. Pires, A. Carvalho and M. B. de Carvalho, *Micropor. Mesopor.*

Mater., **43**, 277 (2001).

25. T. J. Pinnavaia, A. Galarneau and A. Barodawalla, *Nature*, **374**, 529 (1995).

26. M. A. Lillo-Ródenas, D. Cazorla-Amorós and A. Linares-Solano, *Carbon*, **43**, 1758 (2005).

27. S. K. Modak, A. Mandal and D. Chakrabarty, *Polym. Composite*, **34**, 32 (2013).

28. Y. Wang, P. Zhang, K. Wen, X. Su, J. Zhu and H. He, *Micropor. Mesopor. Mater.*, **224**, 285 (2016).

29. K. Kwon, W. Jo, H. Lim and W. Jeong, *J. Hazard. Mater.*, **148**, 192 (2007).

30. J. A. Park, J. K. Kang, J. H. Kim, S. B. Kim, S. Yu and T. H. Kim, *Environ. Eng. Res.*, **20**, 133 (2015).

31. Y. Hu, L. Liu, F. Min, M. Zhang and S. Song, *Colloids Surf., A*, **434**, 281 (2013).

32. K. Kosuge, S. Kubo, N. Kikukawa and M. Takemori, *Langmuir*, **23**, 3095 (2007).

33. K. S. W. Sing, *Pure Appl. Chem.*, **57**, 603 (1985).

34. H. Chen and D. A. Schiraldi, *Polym. Rev.*, **59**, 1 (2019).

35. Q. Guo, Y. Liu, G. Qi and W. Jiao, *Chem. Eng. Res. Des.*, **143**, 47

36. A. Amari, M. Chlendi, A. Gannouni and A. Bellagi, *Appl. Clay Sci.*, **47**, 457 (2010).

37. J. Benkhedda, J. Jaubert, D. Barth and L. Perrin, *J. Chem. Eng. Data*, **45**, 650 (2000).

38. C. Wang, K. Chang, T. Chung and H. Wu, *J. Chem. Eng. Data*, **49**, 527 (2004).

39. M. A. Lillo-Ródenas, A. J. Fletcher, K. M. Thomas, D. Cazorla-Amorós and A. Linares-Solano, *Carbon*, **44**, 1455 (2006).

40. J. Zhang, S. Lu, J. Li, P. Zhang, H. Xue, X. Zhao and L. Xie, *Energies*, **10**, 1586 (2017).

41. I. Ushiki, M. Ota, Y. Sato and H. Inomata, *Fluid Phase Equilib.*, **375**, 293 (2014).

42. B. Azambre, A. Westermann, G. Finqueneisel, F. Can and J. D. Comparot, *J. Phys. Chem. C*, **119**, 315 (2015).

43. I. Ushiki, M. Ota, Y. Sato and H. Inomata, *Fluid Phase Equilib.*, **344**, 101 (2013).

44. N. Takahashi, I. Ushiki, Y. Hamabe, M. Ota, Y. Sato and H. Inomata, *J. Supercrit. Fluids*, **107**, 226 (2016).

(2019).